Nano Energy 129 (2024) 109956

Contents lists available at ScienceDirect

Nano Energy

journal homepage: www.elsevier.com/locate/nanoen

Machine learning enhanced rigiflex pillar-membrane triboelectric nanogenerator for universal stereoscopic recognition☆

Yao Xiong [a,b], Yang Liu [a,b], Jiahong Yang [a,b], Yifei Wang [a,b], Nuo Xu [a,c], Zhong Lin Wang [a,d,*], Qijun Sun [a,b,c,e,*]

[a] Beijing Institute of Nanoenergy and Nanosystems, Chinese Academy of Sciences, Beijing 101400, PR China
[b] School of Nanoscience and Technology, University of Chinese Academy of Sciences, Beijing 100049, PR China
[c] Center on Nanoenergy Research, School of Physical Science & Technology, Guangxi University, Nanning 530004, PR China
[d] Georgia Institute of Technology, Atlanta, GA 30332, USA
[e] Shandong Zhongke Naneng Energy Technology Co., Ltd, Dongying 257061, PR China

ARTICLE INFO

Keywords:
Triboelectric nanogenerator
Machine learning
Rigiflex
Active sensor
Stereoscopic recognition

ABSTRACT

The advent of the artificial intelligence (AI) and Internet of Things (IoTs) era has spurred a surge in the analysis of voluminous data gathered from myriad distributed sensors. This endeavor is primarily aimed at executing sophisticated recognition functions, which frequently demand excessive energy consumption. As a result, the development of a streamlined design capable of performing these functions with comparable efficiency continues to pose a significant challenge. Herein, a rigiflex pillar-membrane triboelectric nanogenerator (PM-TENG) is proposed for universal stereoscopic recognition by machine learning. An integral design is adopted to generate dynamic sensing signals in time series, which can obtain abundant and high-resolution information of stereoscopic structures. By combining the advantages of both rigid steel pillars and flexible/elastic membranes, the proposed rigiflex PM-TENG contains information from multiple sensing pillared pixels and focuses on the study of dynamic changes during the whole contact cycle. The proposed rigiflex TENG can effectively recognize objects across nine categories by leveraging machine learning technique, achieving an accuracy rate of 96.39 %. This system offers substantial potential for application in assembly lines for production control management in future smart factories and unattended warehouse workshops.

1. Introduction

The rapid advancement of artificial intelligence (AI) and 5 G technology is ushering in a new era for Internet of Things (IoTs). These cutting-edge technologies hold the potential to revolutionize intelligent manufacturing and smart home systems. Leveraging the IoT framework to couple with extensive data transmission capabilities facilitates real-time sensory information gathering, data management, and analysis [1]. The integration of AI and IoT technologies paves the way for an AI-centric living, working, and manufacturing environment, termed as AI of Things (AIoTs). This integration promises streamlined IoT operations, augmented human-machine interaction, and enriched decision-making processes that are dynamic and systematic [2]. With the pervasive sensor data from AIoTs, real-time control and optimization of products and production lines can be readily achieved.

Over the past few decades, a proliferation of sensory devices, grounded in materials sciences, has been developed using micro/nano-fabrication technology. These devices have found applications in areas such as environmental detection [3–7], motion monitoring [8–10], and intelligent control [11–15]. Concurrently, numerous sensing mechanisms have been extensively researched. These include resistive-based, capacitive-based, and transistor-based sensors designed to detect strain, static/dynamic force, or even complex motions with high sensitivities [16–18]. Despite advancements in sensor sensitivity achieved through these studies, certain limitations continue to restrict their practical applications. Currently, most sensor functions rely on

☆ Prof Zhong Lin Wang, an author on this paper, is the Editor-in-Chief of Nano Energy, but he had no involvement in the peer review process used to assess this work submitted to Nano Energy. This paper was assessed, and the corresponding peer review managed by Professor Chenguo Hu, also an Associate Editor in Nano Energy

* Corresponding authors at: Beijing Institute of Nanoenergy and Nanosystems, Chinese Academy of Sciences, Beijing 101400, PR China.
E-mail addresses: zhong.wang@mse.gatech.edu (Z.L. Wang), sunqijun@binn.cas.cn (Q. Sun).

https://doi.org/10.1016/j.nanoen.2024.109956
Received 26 May 2024; Received in revised form 29 June 2024; Accepted 1 July 2024
Available online 6 July 2024

time-domain data analysis of the collected sensing signals, typically through frequency and signal amplitude analysis, with an emphasis on enhancing sensitivity and signal mapping [19,20]. However, traditional methods of sensory signal analysis may inadvertently omit some significant features within the sensing signals.

The swift advancement of machine learning (ML) paves the way for enhancing sensor functionality through a specific method of signal analysis and processing [21]. To extract detailed sensory information from these sensors, sophisticated AI technology employing ML-assisted data analytics can be utilized in a monitoring or recognition system. This approach eliminates the need to expend significant energy to upgrade the hardware performance of the sensory equipment. By leveraging appropriate learning models for the specific sensing applications, more detailed and comprehensive information can be extracted from the simply designed sensors, such as contact force, contact sequences, and approaching speed [22–25]. The output patterns trained from the touching or contacting behavior subjected to various objects/motions/structures and relevant recognition process can be achieved, rather than simple state detection [26–30]. Therefore, machine learning offers a promising and feasible solution for achieving high accuracy with low computational cost in ubiquitous sensors. The advancements in highly adaptive machine learning techniques hold potential for an economical and feasible solution for future practical applications such as smart factory and intelligent manufacturing.

The analysis of vast data gathered from numerous distributed sensors is becoming increasingly prevalent [20,31–33]. A scalable tactile glove system, equipped with a sensor array of 548 distributed sensors and assisted by deep convolutional neural networks, was developed to identify individual objects, estimate their weights, and investigate the typical tactile patterns observed during object grasping [34]. Higher resolution in sensing array typically correlates with an increase in the number of sensing pixels and electrodes, leading to higher costs and complexities in structure design, fabrication, data collection, and signal processing [31,35]. The substantial volume of generated data, which demands increased computing power, may not be essential for all standard interactive applications. To address this issue, the concept of minimalist design was introduced [36–38]. This trend generally aligns with the application of in-sensor machine learning processing. For instance, Boutry et al.[39] reported on a bioinspired e-skin deployed on robotic finger that primarily utilized a multi-dimensional capacitive sensor, adhering to the minimalistic concept. The proposed e-skin can detect both normal and shear forces with high sensitivity, demonstrating precise hand dexterity information. This research could potentially enhance the design of sensory systems in soft robotics. Accordingly, common requirements on the minimalist sensor design include achieving the same functionality as multiple sensing arrays using a minimal number of sensing units or even a single unit [40,41]. Besides, minimalist-designed sensors paired with proper machine learning models are highly desirable to detect time-series contact patterns/sequences.

Since its inception in 2012, the triboelectric nanogenerator (TENG) has garnered significant global attention as an effective high-entropy energy harvesting technology [42]. This is due to its high output performance, wide availability of materials, lightweight nature, ease of manufacturing, simple configuration, diverse operation modes, and cost-effectiveness. Beyond energy harvesting, TENGs can function as various types of sensors, offering a promising approach to self-powered spatiotemporal sensing that is crucial for reducing overall system power consumption and endowing multimodality. They can serve as self-powered sensors for a variety of mechanical stimuli, including dynamic pressure/tactile sensing [43,44], vibration detection by rigid-flexible coupling design [11,45–47], acoustic [48,49]/speed [50]/human motion monitoring [51], biomedical sensors [9], and artificial afferents [52,53]. Despite extensive research on TENGs across a range of applications, most studies focus on planar structures with contact-separation mode. Research on stereoscopic objects' contact-separation has been minimal, resulting in few TENG tactile sensors capable of stereoscopic sensing [54]. Therefore, the development of a TENG-based self-powered object recognition system could offer an energy-efficient solution for future intelligent interaction and manufacturing. At present, visual recognition represents one of the most advanced methods for achieving recognition tasks, such as facile feature identification and human motion capture. However, these technologies exhibit several limitations in their applications. For instance, visual recognition has difficulty detecting fine features and is not effective in dark environments, thereby limiting its use at nighttime [55,56]. Consequently, TENG-based sensors could serve as a crucial complementary solution to visual recognition, particularly considering energy conversation. When integrated with the recently popular ML technique, it holds potential to identify the shape, size (or even type) of objects (or components) for classification purposes in unattended factories.

In this study, we introduce a rigiflex pillar-membrane triboelectric nanogenerator (rigiflex PM-TENG) enhanced with ML technique for universal stereoscopic recognition. Drawing parallels to the Yin-Yang complementarity found in Tai Chi (Fig. 1**a-i**), the designed PM-TENG adeptly merges the benefits of rigid/compact pillared structures mounted against a flexible/elastic membrane, termed "rigiflex", which ensure that the rigidity maintains the sensing position while retaining flexibility for an adaptive sensing process [57]. In this design, the rigid μm-scale steel pillar structure is utilized to discern the object's stereoscopic shape as reflected by the corresponding displacements of steel pillars. The dense distribution of steel pillars on the supporting board facilitates high-fidelity sensing of the object (Fig. 1**a-ii**). All the rigid steel pillars are interconnected with the Al tape electrode to achieve minimalistic sensing. The flexible membrane allows the rigid steel pillars to revert to their initial state, simplifying repeated experiments (Fig. 1**a-iii**). Our proposed rigiflex PM-TENG encompasses data from multiple sensing pillars, emphasizing the examination of the dynamic changes throughout the entire contact cycle. To broaden the capabilities of the TENG-based minimalistic sensor, ML techniques enable complex tasks using the sensory data in the time domain, such as object recognition. Furthermore, we have successfully constructed a real-time object recognition system by integrating the minimalistic-designed rigiflex PM-TENG with advanced ML-based data analytics. This system comprises four stages: dynamic sensing, triboelectric signal acquisition, artificial neural network (ANN) model training, and object recognition (Fig. 1**b**), which enables the integral, minimalistic design to generate dynamic sensing signals in time series and offering rich/detailed spatiotemporal information on stereoscopic recognition. In essence, our TENG-based self-powered object recognition system offers an energy-efficient solution. This serves as a complementary element to visual recognition, paving the way for future intelligent interaction and manufacturing processes. These include object recognition, intelligent sorting, and recycling or reproducing incorrect products in smart factory (Fig. 1**c**).

2. Results and discussions

2.1. Design, working mechanism, and characterization

The schematic structure of the rigiflex PM-TENG is delineated in Fig. 2**a**. This configuration consists of six distinct components: steel pillars, a plastic support plate, an Al electrode, a flexible membrane, fixing bolts, and an acrylic baffle (Fig. S1, S2). The Al electrode is interconnected with all the steel pillars. We have chosen highly elastic nitrile rubber (NBR) as the flexible membrane material (Fig. S3), which is affixed to the support plate on all four sides. Notably, each steel pillar can be displaced along its axial direction. By employing a μm-scale pillar structure, we can discern the curvature of an object by observing the displacements of these steel pillars. The dense arrangement of steel pillars on the support plate (with precisely confined positions by laser-engraved holes) facilitates high-fidelity sensing of the object. The

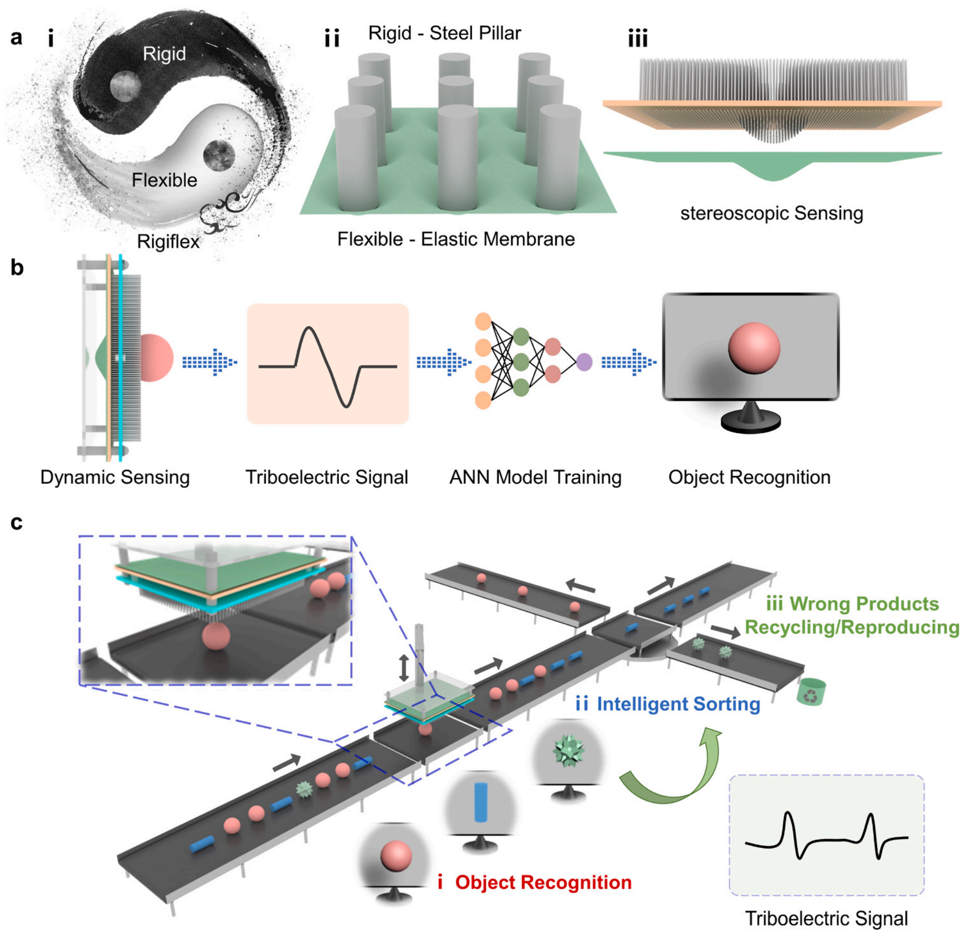

Fig. 1. The schematics and prospects of the rigiflex PM-TENG. (**a**) The structure of rigiflex PM-TENG sophisticatedly combining the advantages of both rigid steel pillars and flexible elastic membrane, which is analogy to the complementarity of Yin-Yang in Tai Chi. (**b**) The process of realizing object recognition leveraging ML techniques, including dynamic sensing, triboelectric signal acquisition, ANN model training and object recognition. (**c**) The potential applications in an assembly line for production control management in next-generation smart factories and workshop management at unattended warehouses.

comprehensive dimensions of the rigiflex PM-TENG are provided in Fig. 2**a**. In contrast, only the rigid steel pillars cannot revert to their original state (Fig. S4a), while the sole flexible/elastic membrane encounters difficulties achieving fully conformal contact, particularly with objects possessing sharp stereoscopic shapes (Fig. S5).

In the proposed rigiflex PM-TENG, the triboelectric output is derived from the contact electrification during the surface interaction between two dissimilar materials. Consequently, in comparison to conventional inertial sensors, triboelectric-based sensors that produce self-generated signals can significantly reduce power consumption [15,58]. The working mechanism of the rigiflex PM-TENG is schematically illustrated in Fig. 2**b**. Typically, a triboelectric sensor exhibits two contrasting pulse waveforms, corresponding to either a contact or separation cycle, contingent on which side the output signal is extracted. In the proposed rigiflex PM-TENG based stereoscopic sensor, it operates based on the interaction between the sensory device and external object. Initially, the stereoscopic sensor and the target object are separated by a specific distance. The inherent insulating property of the polytetrafluoroethylene (PTFE) coated on the object allows for the confinement of induced electrostatic charges with opposite signs on its surface over an extended period. As the object approaches the steel pillars, a decrease in distance results in the Ag electrode on object having a higher electric potential than the Al electrode. This causes electrons to be drawn from the Al electrode to the Ag electrode, generating a positive output current signal. As the object continues to approach, some portion of it will make contact with the steel pillars while the remainder remains in the approaching state. This means that the current signal will continue to generate until the object fully contacts the steel pillars. When the object begins to separate from the device, the electrons from the Ag electrode are compelled to flow towards the Al electrode due to the induced electrical potential difference between them, resulting in a negative output current signal. To validate this proposed mechanism, potential distributions under the open-circuit conditions are simulated using COMSOL software, as illustrated in Fig. S6.

To further illustrate the efficacy of the proposed rigiflex PM-TENG, a comparative test is conducted among the traditional TENG with flexible membrane (M-TENG), the pillar-structured TENG without membrane (P-TENG), and the proposed rigiflex PM-TENG when subjected to a spherical object (Fig. 2**c-e**). The signals from M-TENG (short-circuit current I_{SC} = 17.9 nA, open-circuit voltage V_{OC} = 8.3 V, short-circuit charge Q_{SC} = 1.56 nC) are significantly smaller than those from both P-TENG and the rigiflex PM-TENG. This suggests that the conventional M-TENG is unsuitable for object sensing due to its limited contact area. However, the μm-scale movable pillar structure allows devices with steel pillars to fully engage with the object, thereby significantly expanding the contact area. Notably, the signals from rigiflex PM-TENG in response to a spherical object are higher than those from P-TENG, attributed to the flexible membrane's elasticity. With the flexible/elastic membrane, the rigiflex PM-TENG enables more complete contact between the steel pillars and the object, even under some degree of compression. Beyond signal enhancement, the flexible/elastic membrane also plays a crucial role in the restoring of the steel pillars, facilitating multiple and

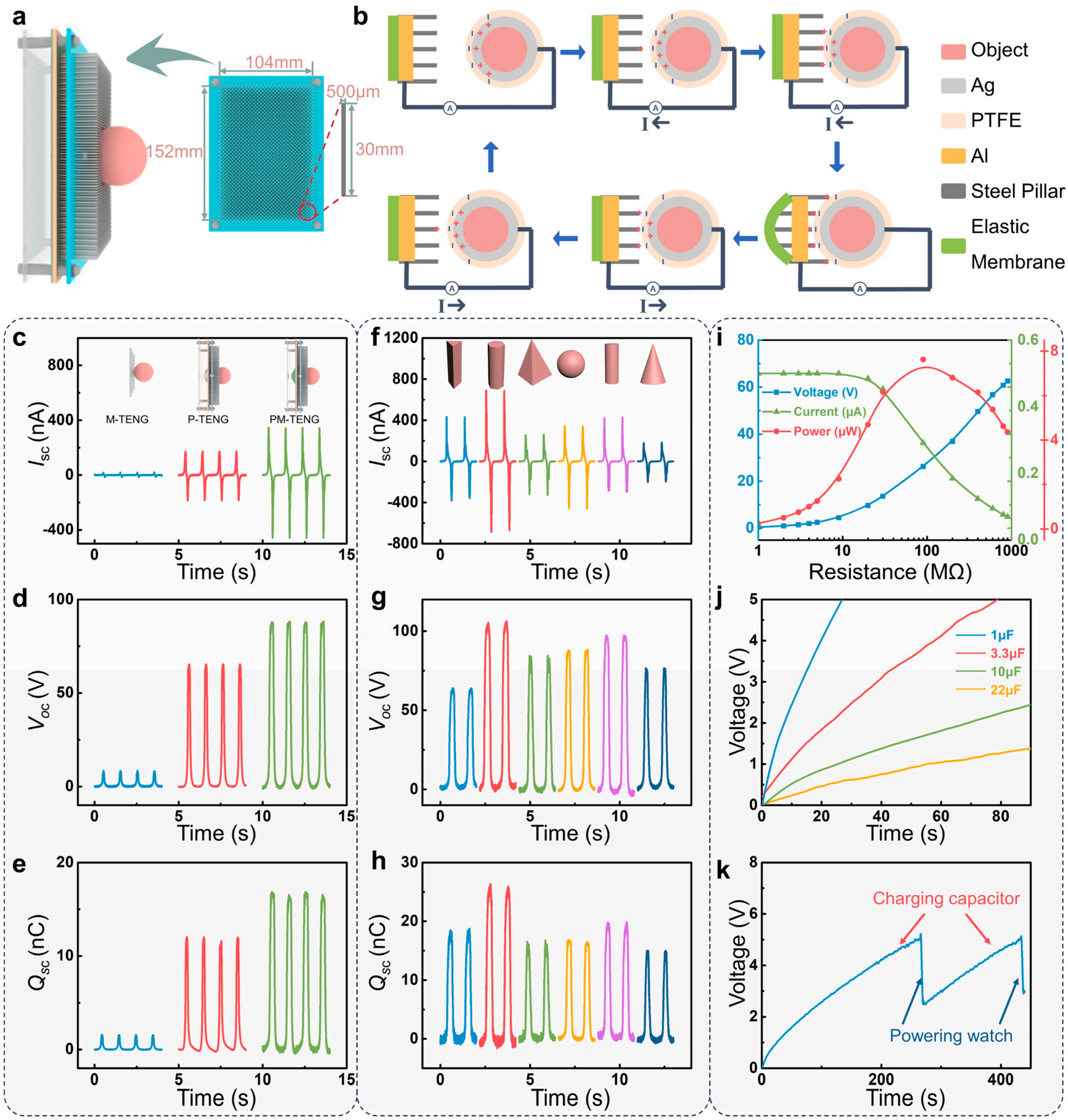

Fig. 2. The schematic structure, working mechanism, and characterization of the rigiflex PM-TENG. (**a**) The schematic structure and the detailed dimensions of the rigiflex PM-TENG. (**b**) The working mechanism of the rigiflex PM-TENG which works in contact-separation mode. (**c-e**) Electrical outputs of the M-TENG, P-TENG, and rigiflex PM-TENG against the sphere-shaped object, which include the short-circuit current (I_{SC}), the open-circuit voltage (V_{OC}) and the transferred charges (Q_{SC}). (**f-h**) Electrical outputs of the rigiflex PM-TENG against objects with various stereoscopic shapes. (**i**) Dependence of the output voltage, current, and power on the external load resistance. (**j**) Charging curve of different commercial capacitors (i.e., 1, 3.3, 10, and 22 μF). (**k**) Charging and discharging curve with the rigiflex PM-TENG, where each voltage drop represents a discharging to the electronic watch.

repeatable object recognition. Utilizing the rigiflex PM-TENG structure, electrical outputs against objects of various shapes are also enhanced, as illustrated in Fig. 2**f-h**. Interestingly, while signals from rigiflex PM-TENG against objects of various shapes display different peak values, signal peaks from P-TENG against similar objects are remarkably close (Fig. S4c-**e**, corresponding triboelectric potential simulation in Fig. S7). The projection areas of all objects partially entering the device are nearly identical, resulting in closely similar signal peaks among different objects tested with P-TENG. However, incorporating an elastic membrane into the rigiflex PM-TENG would induce compression between the objects and steel pillars. The variability of the invasive degree and contact force in time series can be clearly reflected among different objects during the contact and partial entry process. A comparative analysis of three devices reveals that the rigiflex PM-TENG is optimal for precise object sensing. Corresponding durability tests of the rigiflex PM-TENG are also illustrated in Fig. S8.

As a supplementary advantage, the rigiflex PM-TENG can also be utilized as an energy harvester to harness waste energy from contact motion. At a frequency of 1 Hz, a peak power of 7.63 μW is recorded with load resistor of 90 MΩ (Fig. 2**i**). The rectified output voltages from the rigiflex PM-TENG could successfully charge various capacitors of 1, 3.3, 10, and 22 μF to achieve a voltage of 5 V (Fig. 2**j** and Fig. S9a), thereby illustrating its robust charging capability as a dependable power source. Within approximately 250 seconds, the output from the rigiflex PM-TENG could charge a 22 μF capacitor up to 5 V, sufficient to continuously power up a commercial electronic watch (Fig. 2**k**, Fig. S9b).

2.2. Dynamic sensing mechanism of the rigiflex PM-TENG

The dynamic sensing mechanism of the rigiflex PM-TENG, designed to detect objects of varying shapes, is illustrated in Fig. 3. This approach diverges from other strategies that utilize numerous distributed pressure sensors, which primarily analyze the mapping of the static sensing signals for differentiation. Instead, our experiment employs an integral, minimalistic design to generate dynamic sensing signals in time series, which can deliver rich and detailed spatiotemporal information on various stereoscopic structures. The proposed rigiflex PM-TENG offers a cost-effective solution with reduced multiplexing and computational requirements compared to distributed sensory matrix [34]. The typical dynamic sensing process is depicted in Fig. 3**a-i**, comprising three main stages: approaching, contacting, and partially invasive process. Notably, during the partially invasive stage, the steel pillars in the rigiflex PM-TENG are dynamically and gradually displaced backward, ensuring the complete replication on the feature shapes of the objects.

In this manner, the shapes of different objects can be represented by the dynamic displacements of the dense steel pillars, which are reflected in temporally characterized dynamic current signals. Even when objects are invasive in the sensory device only partially, their most distinctive characteristics are fully captured. The use of dense steel pillars allows the device to perceive significant segment information about the objects, implying that each steel pillar carries continuous shape information according to their corresponding contact position. Additionally, the laser-engraving Al electrode plays a crucial role in connecting all the steel pillars, which is vital for our integral and minimalist design. The combined signals effectively reflect key shape features such as the object curvature, contact area, contact sequence, and position. Apart from the rigid steel pillars, the flexible/elastic membrane against the rigid pillars can ensure the adaptive deformation and enable the rigid steel pillars to revert to the initial state, thereby facilitating successive and repeated object recognition, e.g., on the factory/logistics assembly line.

The 3D exploded view of the rigiflex PM-TENG in relation to a spherical object is depicted in Fig. 3**a-ii**, providing an intuitive representation of the displacements experienced by the steel pillars and the deformation observed in the flexible membrane. To elucidate the signal sequence during the sensing process, we also examine specific objects with noncontinuous shapes (e.g., objects with multilevel structures). As shown in Fig. 3**b**, the 3D exploded views deliver the rigiflex PM-TENG against different objects with single-level, dual-level, and triple-level structures. The temporal contact sequence can be intuitively discerned

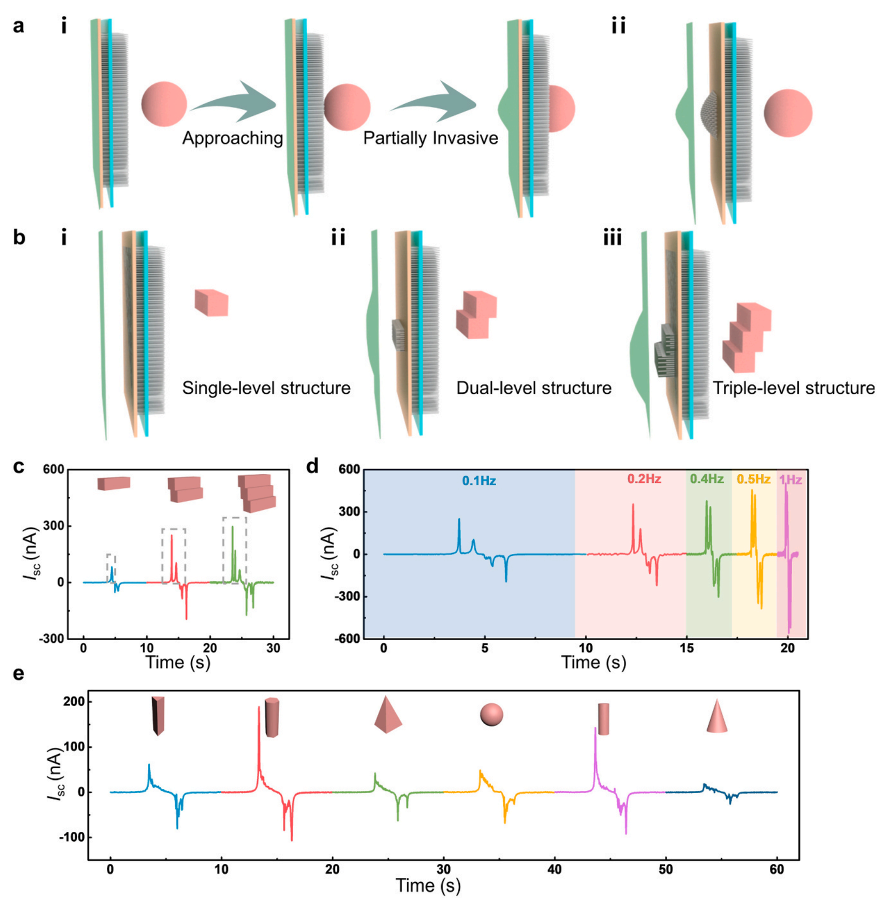

Fig. 3. Dynamic sensing mechanism of the rigiflex PM-TENG against objects with various shapes. (**a**) (**i**) The dynamic sensing process for the sphere-shaped object, consisting of approaching, contacting, and partially invasive process. (**ii**) The 3D exploded view of the rigiflex PM-TENG against the sphere-shaped object showing the displacements of the steel pillars and the deformation of the membrane. (**b**) The 3D exploded view of the rigiflex PM-TENG against single level (**i**), dual levels (**ii**), triple levels (**iii**). (**c**) The sensing signals corresponding to single level, dual levels, and triple levels illustrating shape-related variations during the sensing process. (**d**) The sensing signals for two levels at various frequencies (0.1, 0.2, 0.4, 0.5, and 1 Hz). (**e**) The sensing signals corresponding to different objects.

based on the sensing process when dealing with the multilevel shaped objects, as there exists a time interval between these layers. The corresponding sensing signals for single-level, dual-level, and triple-level are illustrated in Fig. 3**c**. The sensing peaks are observed to be sequentially generated, indicating the multilevel contact patterns in the time domain. Notably, the number of peaks corresponds to the level numbers within objects, while objects with continuous and uniform shape exhibit only a single peak. This means that a single-level structure will produce one peak, a dual-level structure will produce two peaks, and a triple-level structure will produce three peaks. The number of peaks corresponds to the number of discontinuous layers. Consequently, the number of signal peaks serve as an effective means to distinguish the objects with multilevel and noncontinuous shapes, whose variation arises from the differing contacting surfaces associated with single-/dual-/triple-level structure. We further explore the impact of frequency on sensing signals, as depicted in Fig. 3**d**. Our primary focus is on the sensing signals for the dual-level shaped objects at varying frequencies (0.1, 0.2, 0.4, 0.5, and 1 Hz). As the contact frequency escalates from 0.1 to 1 Hz (with a contact-separation distance of 86 mm), the peak value rises from 251 to 503 nA. Additionally, the disparity between the two sensing peaks gradually decays, attributed to the more transitory contact between the two levels in the objects with the increasing contact frequency.

Notably, similar to the signals associated with objects of multilevel structures, those objects of continuous and uniform shapes also encapsulate a wealth of temporal shape information. However, the key distinction lies in the manner these temporal signals are presented: while they are entirely distinct for multilevel structured objects, they are superimposed for those of continuous shape. Fig. 3**e** illustrates the sensing signals corresponding to various continuous-shape objects. Although it is not possible to discern individual objects from these signals directly, the intricate details of each object are evident within the time domain of the sensing signal (Fig. S10). A comparative analysis of the signals from different shapes reveals that an object's curvature directly influences its signal reduction speed; objects with greater curvature exhibit slower signal decay. Thus, the dynamic sensing capabilities of an object by the rigiflex PM-TENG, irrespective of the target shape, are manifested in its signal reduction rate (crucial for subsequent characteristic extraction by ML method).

2.3. Data processing and classification performance via machine learning

Machine learning technique serves as an effective method for addressing classification problems characterized by complex input signals. It facilitates the automatic extraction of features from the datasets using specific algorithms, such as principal component analysis (PCA), locally linear embedding (LLE) to enhance subsequent object recognition [55,56]. The aforementioned research underscores the ability of the proposed rigiflex PM-TENG to discern detailed and rich information about objects. In the following study, we employ a shape-related signal, augmented by machine learning, for object classification. We have selected nine objects of varying shapes for identification, recording the triboelectric outputs from the contact process involving triangular prisms, hexagonal prisms, pyramids, spheres, cylinders, cones, single-/dual-/triple-leveled shapes. Current recognition strategies for triboelectric outputs predominantly analyze intricate features within a single waveform, such as frequency, hold time, latency, and peak gaps. This approach fails to recognize complex features with subtle differences and is highly sensitive to environmental variations, leading to diminished recognition accuracy. To solve these problems, our approach leverages a minimalistic sensor that captures rich temporal characteristics during the contact process. This provides ample features before automatic extraction using machine learning. Consequently, raw data from a dynamic contact process—including contact position, force, speed, area, and sequence—can be input into the training model.

Among various ML methodologies, the artificial neural network (ANN) stands out as a highly effective supervised learning model used for classification tasks [2,25]. It has been proposed for use in analyzing triboelectric output signals with superior performance. The ANN model presents a promising and practical solution for time-domain sensor data analysis. Consequently, we have constructed a custom ANN-based analytic system to facilitate object classification (Fig. S11, Table S1). As depicted in Fig. 4**a**, we have designed a four-layer ANN model comprising an input layer, two hidden layers, and an output layer. The input layer corresponds to the sensor data with time sequences, while the output layer corresponds to the true labels of objects with diverse shapes. Each sample's sensor data length is 2000. In this process, sensor data from nine objects of varying shapes—including triangular prism, hexagonal prism, pyramid, sphere, cylinder, cone, single-/dual-/triple-leveled objects—are collected accordingly by repeating approaching, contact, and partially entering motions. Notably, the contacting position of each test may vary slightly, ensuring that the data collection process closely aligns with real-world scenarios. We directly utilize the raw current data in time domain of rigiflex PM-TENG as sample features, resulting in 2000 features for each sample. Each feature represents one data point in the time series during the contact process. To ensure the reliability of the dataset during data collection, each object is tested 200 times. The 1800 samples across nine categories are then randomly divided into two groups: training samples (80 %) and testing samples (20 %).

Fig. 4**b** illustrates the typical triboelectric outputs from contacting all nine objects at varying frequencies (0.1, 0.2, 0.4, 0.5, and 1 Hz). These results are distinct from other reported devices that utilize dense resistive sensors arrays and employ ANN to evaluate the mapping of the static sensing signals during object contact activities. In contrast, the proposed rigiflex PM-TENG device with a minimalistic sensor incorporates information from the integral and dense sensing pillars, more emphasizing the investigation of the dynamic changes throughout the entire contact cycle. Initially, the multiple steel pillars of rigiflex PM-TENG are aligned. As the object of specific shape interacts with these steel pillars, the corresponding forced steel pillars adaptively displace following the shape of the target object. Eventually, the shape of the dense steel pillars aligns well with the object's shape, indicating that the rigiflex PM-TENG can readily replicate and detect the object's specific shape. The target object's shapes result in different displacement states for each steel pillar, generating dissimilar waveforms to distinguish different objects.

According to the above discussions, the triboelectric output signal effectively reflects the temporal variations in the contact area between the object and the multiple steel pillars, specifically, the curvature of the object. This is crucial for achieving accurate object recognition. Due to the substantial dimensions of acquired data samples, each sample consists of 2000 elements. To extract the features and reduce data dimensions, we utilize the PCA method, employing a kernel function as the linear function. The minimum proportion threshold of the variance sum of the principal components (referred to as n_components) is set at 0.99. This adaptive determination of the number of dimensions to be reduced ensures that the processed data retains at least 99 % of the original sensor data information.

The recognition accuracy is mainly affected by the data discrepancy among different labels and the constructed ML model. Similar sensing signals may lead to probable misrecognition on the target objects. In order to compare the performance of different ML models based on the rigiflex PM-TENG sensor data to further optimize the capacity on object recognition, we have also constructed a support vector machine (SVM) model (Table S2) [59], which is another widely utilized machine learning method. Generally, the SVM model demonstrates superior accuracy in recognizing small datasets rich in distinguishable features. Conversely, the ANN model typical excels when handling large amounts of data with similar patterns due to its ability to automatically extracting significant features. Within the SVM model, two parameters play a crucial role in determining the appropriate model: the penalty coefficient C and kernel coefficient gamma (γ). These coefficients are used to

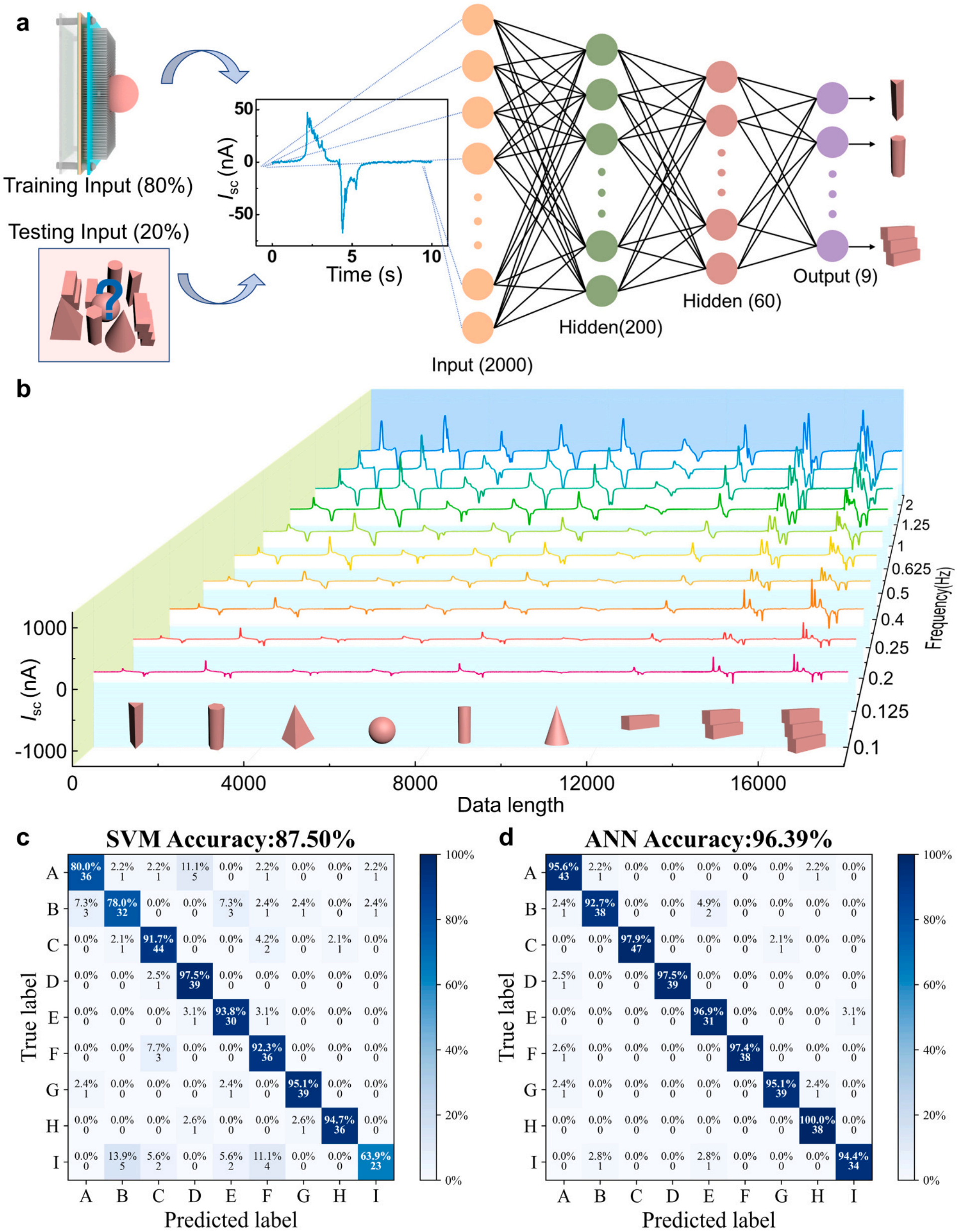

Fig. 4. Triboelectric output-based object recognition leveraging machine learning technique. (**a**) Schematics of the process and parameters for constructing the ANN model. (**b**) Triboelectric outputs corresponding to different objects. (**c-d**) Confusion maps of object recognition derived from two models made by SVM (c) and ANN (d) with 360 test samples. Predicted label refers to the recognized result, and true label refers to the true object. A, B, C, D, E, F, G, H, and I represent triangular prism, hexagonal prism, pyramid, sphere, cylinder, cone, single-level, dual-levels, and triple-level shapes, respectively.

assess the potential for misclassification. The confusion maps for the optimized SVM model and the optimized ANN model are illustrated in Fig. 4**c** and **d**, respectively. The proposed ANN model demonstrates a significant improvement over the SVM model, assisting rigiflex PM-TENG to achieve an accuracy of 96.39 % in object recognition using only 360 training samples (Fig. 4**d**). In contrast, the SVM model only achieves an accuracy of 87.5 % (Fig. 4**c**). This disparity is attributed to the superior suitability of the ANN model (better than SVM model) for our specific object classification task based on the rigiflex PM-TENG sensing data. Our experimental results suggest that both the recognition models developed from ANN and SVM methods perform satisfactorily. However, the proposed ANN model outperforms the SVM model, indicating its suitability for our problem domain. Given the advanced automatic feature extraction capabilities of the ANN method, the proposed rigiflex PM-TENG only necessitates a relatively simple network to achieve high performance.

Notably, the accuracy is mainly affected by the data discrepancy among different labels. The more similar the data, the more likely it is to be confused. Besides, a limited number of classes exhibit relative lower accuracy, such as the 92.7 % accuracy for hexagonal prisms in the ANN model (Fig. 4**d**). This indicates two hexagonal prisms incorrectly classified as "cylinder" and one hexagonal prism erroneously identified as "triangular prism". Upon examining the structures of these objects and the triboelectric output patterns depicted in Fig. 4**b** and Fig. S10, several similarities emerge. The triangular prism, hexagonal prism, and cylinder all possess characteristic features of typical prisms; however, their primary structural difference lies in curvature. Varying curvatures lead to dynamic changes in the contacting area and force, resulting in the discrepancies in peak values and the signal reduction speed. Abnormalities in these parameters can lead to incorrect judgments. Therefore, during the data collection phase, augmenting the sample population and adjusting the contacting force are effective strategies to ensure the model stability, even when irregular signals are present. Additionally, modifying the contact position is crucial for enhancing the model's generalization capability. The parameter optimization process of ANN model is shown in Fig. S12-**14**.

2.4. Real-time object recognition system

To demonstrate the potential of the proposed rigiflex PM-TENG for practical applications, we present a real-time object recognition system capable of facilitating real-time monitoring in a cameraless environment. Upon analyzing the recognition outcomes, additional advanced functionalities can be incorporated, such as intelligent sorting and remanufacturing of incorrect products. The rigiflex PM-TENG offers an energy-efficient solution for components recognition in unmanned warehouses. Thus, capturing sufficient information to differentiate various objects becomes crucial for implementing these applications. Fig. 5**a** illustrates the process flow for establishing this real-time system. During the training phase, signals derived from rigiflex PM-TENG against different objects are collected to form a comprehensive dataset with numerous samples. These time domain signals are then normalized to expedite convergence in the gradient descent algorithm. These normalized feature vectors subsequently serve as inputs for constructing object feature models using supervised learning techniques, specifically PCA and ANN. For real-time identification, a comparable procedure is employed, where real-time signals are directed into the trained ANN model for decision-making. This ANN model leverages a tailored classification algorithm adapted from the Sklearn library, striking an optimal balance between computational complexity and prediction accuracy. It is well-suited for scenario involving a large number of objects and allows for theoretical analysis through a precise probability model, mitigating the risk of overfitting in training sets.

Upon training with the ANN model, a real-time object recognition system is realized, as illustrated in Fig. 5**b** (see also Movie S1). This system presents both the real-time signals (indicated by black dashed boxes) and the corresponding predicted images of the objects (highlighted by red dashed boxes). During operation, objects are randomly chosen for testing; subsequently, these objects are recognized by the trained ANN model based on the input signals obtained from rigiflex PM-TENG. Although our focus is solely on the construction of a real-time object recognition system, this demonstration underscores the potential of employing this comprehensively designed rigiflex PM-TENG to facilitate advanced multipurpose operations. An analysis of the

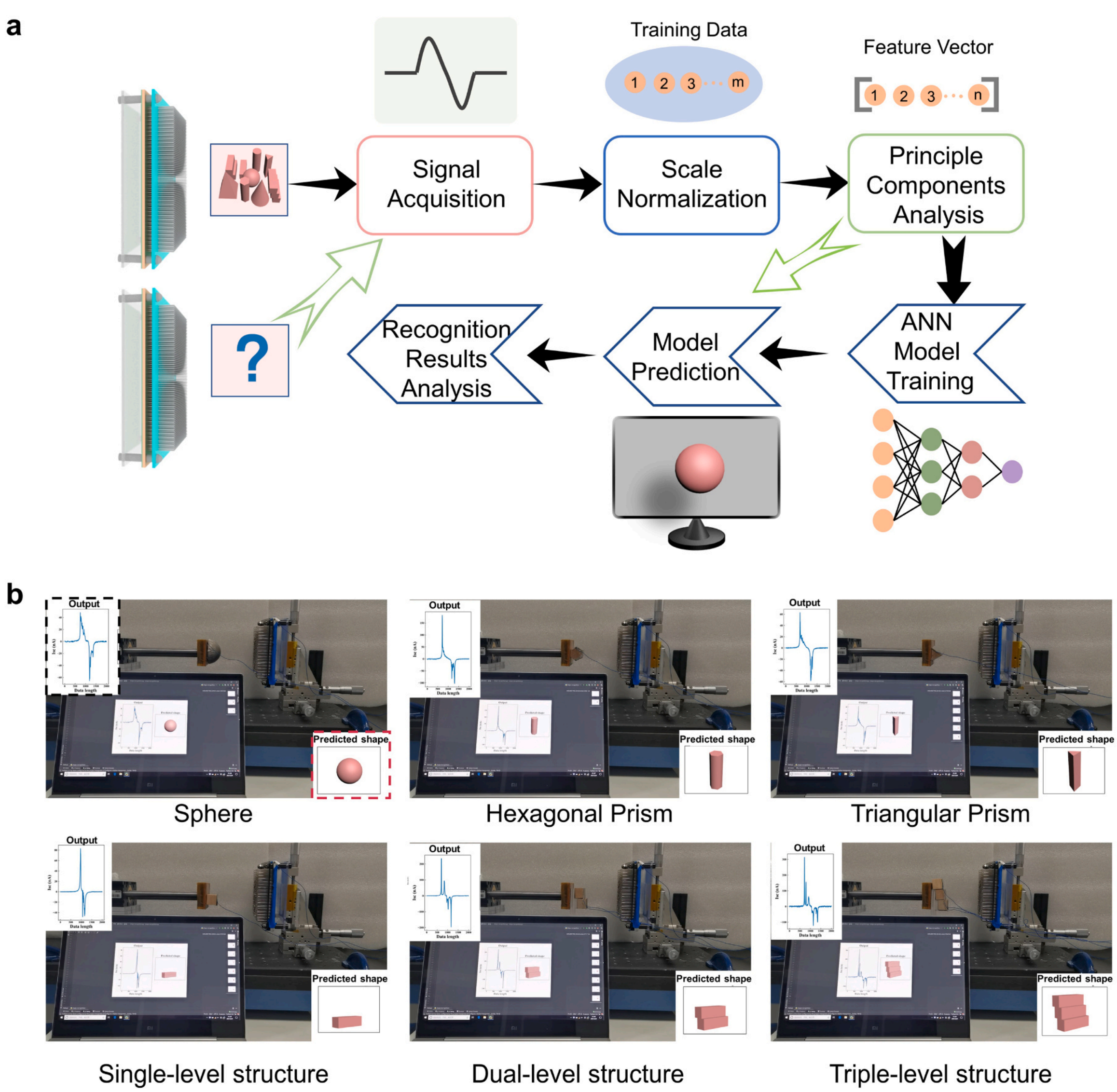

Fig. 5. Real-time object recognition system. (**a**) The process flow of the proposed object recognition system combined with the classification algorithm. The principal component analysis (PCA) is implemented to extract the data feature for ML training based on the ANN model. (**b**) Real-time object recognition system. The screen displays both the real-time signals and the corresponding predicted object's picture.

predicted outcomes suggests that it could potentially enhance intelligent manufacturing, sorting, and production line management. Furthermore, the application of object recognition technology can significantly streamline the entire process.

3. Conclusion

In conclusion, we have successfully demonstrated the utilization of rigiflex PM-TENG for universal stereoscopic recognition by leveraging ML technique. The rigiflex PM-TENG employs an integral and minimalistic structure to generate dynamic sensing signals in time series, providing rich and detailed information on stereoscopic structures. The employed rigid μm-scale steel pillar structure can readily reflect the stereoscopic shape of the objects, as indicated by the corresponding displacements of steel pillars, there enabling high-fidelity object sensing. The flexible membrane allows the rigid steel pillars to revert to their initial state, facilitating repeated experiments. By integrating the benefits of both the rigid steel pillars and the flexible membrane, the proposed rigiflex PM-TENG encompasses information from multiple sensing pixels and emphasizes of the study of dynamic changes throughout the entire contact cycle. Furthermore, a real-time object recognition system has been established with an object recognition over nine categories at an accuracy of approximately 96.39 % by using four layers of the ANN model, which can be further applied to assembly lines for production control management in next-generation smart factories and unattended warehouse's workshop management. This introduced self-powered recognition system holds significant potential as it offers a cost-effective and power-efficient solution for future intelligent interaction and manufacturing processes. As 5 G communication and IoT applications continue to revolutionize human life in various aspects, such device can enhance machine intelligence based on the big data obtained from AI techniques.

Given these advanced capabilities, the rigiflex PM-TENG is poised to revolutionize object recognition tasks across multiple scenarios. The rigiflex PM-TENG, with its unique integration of rigid pillars and flexible membranes, presents a transformative approach to object recognition, applicable across a diverse range of industries. In smart manufacturing, for instance, these sensors could be integrated into robotic arms to enhance the precision and efficiency of automated production lines by enabling the robots to identify and sort materials based on their texture and shape. This capability not only minimizes human error but also boosts production throughput. Similarly, in quality control, rigiflex PM-TENG can detect minute defects or irregularities, ensuring high product quality and customer satisfaction, although it requires careful calibration to avoid false positives. In healthcare, embedding these sensors in prosthetic devices could significantly enhance the functionality by providing tactile feedback, thus improving the quality of life for users, albeit demanding rigorous safety testing. Additionally, in educational settings, these sensors could be used in interactive displays to provide tactile feedback that enriches learning experiences. Moreover, in security systems, rigiflex PM-TENG could add a sophisticated layer of physical security by detecting unique identifiers, enhancing security while raising concerns about privacy. Each of these applications presents its own set of challenges, including integration with existing systems, environmental adaptability, and user acceptance. These issues must be carefully considered to fully exploit the potential of this groundbreaking technology.

4. Experiments

4.1. Fabrication of the rigiflex PM-TENG

For the systematic design of the rigiflex PM-TENG, commercial steel pillars (diameter: 500 μm, height: 30 mm) are selected as the dense and unconventional pixels, and the nitrile rubber is selected as the flexible/elastic membrane material, with its four sides stuck on the Al tape electrode. First, plastic support plate and Al tape electrode are punched to plate with densely aligned holes using a laser-engraving machine. Subsequently, the steel pillars are insert into the corresponding pixel holes on the support substrate. Next, the four sides of the flexible membrane are stuck on the Al electrode. Through fixing bolts, the support substrate, Al electrode and acrylic baffle are fixed.

4.2. Electrical output measurement

To characterize the output properties of the rigiflex PM-TENG, the contact-separation action is applied by a commercial linear mechanical motor. I_{SC}, V_{OC}, and Q_{SC} are measured by an electrometer (Keithley 6514 system). A custom LabVIEW program is used to record the electrical output. In terms of the output voltage, current and power characteristics versus the external load resistance, the output voltages on different loads are measured by a Keithley 6514 Electrometer connected in parallel. Then the peak power on the corresponding external load resistance is calculated using the formula $P = V^2/R$, where P, V, and R are the peak power, output voltage, and resistance of the resistor load, respectively. As for the capacitor charging, the voltages on different capacitors are also measured using the Keithley 6514 electrometer in parallel connection with the capacitors. Analog current signals generated from the rigiflex PM-TENG for real-time object recognition are collected by the Keithley 6514 electrometer. Finite element method simulation of electric potential between two triboelectric layers (polytetrafluoroethylene film covered on object and steel pillars) are numerically simulated using the commercial software COMSOL.

4.3. Data collection and ML training model

The generated triboelectric signals from the rigiflex PM-TENG are acquired by the Keithley 6514 electrometer. In terms of the training data for object recognition, the signal data from each channel is recorded with 2000 data points and 200 samples are collected for each object. A whole dataset is built from 9 objects with various shapes with a total number of 1800 samples. 80 % of the dataset is used for training samples while the rest 20 % is used for test samples. The ANN models used in the system are configured as follows: the categorical cross-entropy function is applied as the loss function, adaptive moment estimation (Adam) is used as the update rule due to its optimization convergence rate; the sigmoid function is used as activation function, and prediction accuracy is used to evaluate the model training. Hyperopt library is applied for serial and parallel optimization on the search space. The ANN models are developed in Python with a Sklearn backend. The feature-based models are trained on a standard consumer-grade computer.

4.4. The architecture and training process of ANN

A four-layer ANN model is constructed, including input layer, two hidden layers, and output layer. The input layer corresponds to the sensor data with time sequences, and the output layer correspond to the true labels of objects with various shapes. The four layers are fully connected via weights. During the training process the weights will be updated via the back-propagation (BP) algorithm whose main idea is to pass the output errors back to the input layer through the hidden layer. By updating the weight of each unit layer by layer, the network output error can be reduced to an acceptable level through error back propagation.

When the sensor data arrives at the input layer, the obtained input vector reaching the first hidden layer (hi_1) is the matrix product of the input sensor data vector (V) and the random initialized weight matrix (W):

$$hi_1 = \sum_{i=1}^{n} w_i v_i$$

The input vector of the first layer (hi_1) is then transformed to the first hidden layer output vector (ho_1) via a sigmoid activation function ($ho_1 = f(hi_1)$):

$$ho_1 = \frac{1}{1 + e^{-hi_1}}$$

The first hidden layer output vector (ho_1) continues to propagate forward through the weights (W_{h1}) connected with the output neurons:

$$hi_2 = \sum_{i=1}^{n} w_{h1i} ho_{1i}$$

Similarly, the second hidden layer output vector (ho_2) can be obtained from the input vector of the second layer (hi_2) via a sigmoid activation function ($ho_2 = f(hi_2)$):

$$ho_2 = \frac{1}{1 + e^{-hi_2}}$$

Then the output vector (Y) can be obtained through the activation function ($Y = f(ho_2)$):

$$Y = \frac{1}{1 + e^{-ho_2}}$$

By comparing the difference between the output value (y) of the output vector and the label value (k) of the input sensor data, ΔW is calculated with the gradient descent method. In this way, all the weights in each layer are updated until the network error meets the precision requirement which is determined by the defined loss function.

4.5. The principle of multi-class SVM

The SVM is originally designed for the two-class (binary) classification. Harnessing the one-against-rest strategy, the two-class SVM is extended to multi-class classification. By switching the customized classifier from the two-class mode to the multi-class mode, the model can serve for more complicated classification and achieve richer functions. One versus rest strategy, one of the multi-class SVM algorithms, is used to classify all the objects. the classification function is constructed between one class and rest classes. In the training process, samples of a certain class are classified into one class with positive labels, and the rest samples are classified into another class with negative labels; hence the samples of k categories construct k SVMs. The sample to be predicted is classified into the class with the largest classification function value. In predicting process, the class with the largest classification-function output will be selected as a prediction class. The specific classification steps are as follows: (1) Pick out all the training samples of object_1 in the object database. (2) Set the samples of object_1 as positive labels and set the rest training samples of other object as negative labels, then use all samples labeled positive and negative as an input to train the SVM_1. In this way, the corresponding SVM_1 and corresponding classification planes are figured out. SVM_1 is used for differentiating object1 from the remaining gestures. (4) Repeat the above steps until the SVM against all the classes are constructed. And we can obtain 9 SVMs: SVM_1, SVM_2, …, SVM_9, and 9 classification planes are obtained. (5) In predicting process, the corresponding test vectors are fed into the 9 training SVM, and acquired a result of $f_1(x)$, $f_2(x)$, …, $f_9(x)$, respectively. Finally, the class with the largest classification-function output will be selected as a prediction class.

CRediT authorship contribution statement

Zhong Lin Wang: Writing – review & editing, Validation, Supervision, Project administration. **Qijun Sun:** Writing – review & editing, Writing – original draft, Validation, Supervision, Project administration, Funding acquisition, Conceptualization. **Nuo Xu:** Investigation. **Jiahong Yang:** Investigation. **Yifei Wang:** Investigation. **Yao Xiong:** Writing – original draft, Visualization, Validation, Methodology, Investigation, Formal analysis, Data curation. **Yang Liu:** Investigation.

Declaration of Competing Interest

The authors declare that they have no known competing financial interests or personal relationships that could have appeared to influence the work reported in this paper.

Data Availability

Data will be made available on request.

Acknowledgements

This work is financially supported by the National Key Research and Development (R&D) Program from Ministry of Science and Technology (2023YFB3208102, 2021YFB3200304), the National Natural Science Foundation of China (52073031), Beijing Nova Program (Z191100001119047, Z211100002121148), Fundamental Research Funds for the Central Universities (E0EG6801X2), and the "Hundred Talents Program" of the Chinese Academy of Sciences.

Appendix A. Supporting information

Supplementary data associated with this article can be found in the online version at doi:10.1016/j.nanoen.2024.109956.

References

[1] R. Krishnamurthy, J. Cecil, A next-generation IoT-based collaborative framework for electronics assembly, Int. J. Adv. Manuf. Tech. 96 (1-4) (2018) 39–52.
[2] R.Z. Shang, H.M. Chen, X. Cai, X. Shi, Y.H. Yang, X. Wei, J. Wang, Y. Xu, Mach. Learn. - Enhanc. Triboelectric Sens. Appl., Adv. Mater. Technol. -Us 2024 (2024) 2301316.
[3] Y. Liu, C. Zhao, Y. Xiong, J. Yang, H. Jiao, Q. Zhang, R. Cao, Z.L. Wang, Q. Sun, Versatile ion-gel fibrous membrane for energy-harvesting iontronic skin, Adv. Funct. Mater. 33 (37) (2023) 2303723.
[4] D. Heo, J. Chung, B. Kim, H. Yong, G. Shin, J.W. Cho, D. Kim, S. Lee, Triboelectric speed bump as a self-powered automobile warning and velocity sensor, Nano Energy 72 (2020) 104719.
[5] C.H. Sun, Q.F. Shi, D. Hasan, M.S. Yazici, M.L. Zhu, Y.M. Ma, B.W. Dong, Y.F. Liu, C. Lee, Self-powered multifunctional monitoring system using hybrid integrated triboelectric nanogenerators and piezoelectric microsensors, Nano Energy 58 (2019) 612–623.
[6] X. Lin, Z. Feng, Y. Xiong, W. Sun, W. Yao, Y. Wei, Z.L. Wang, Q. Sun, Piezotronic neuromorphic devices: principle, manufacture, and applications, Int. J. Extrem Manuf. 6 (3) (2024) 032011.
[7] K. Zhao, B. Ouyang, C.R. Bowen, Z.L. Wang, Y. Yang, One-structure-based multi-effects coupled nanogenerators for flexible and self-powered multi-functional coupled sensor systems, Nano Energy 71 (2020) 104632.
[8] R. Di Giacomo, L. Bonanomi, V. Costanza, B. Maresca, C. Daraio, Biomimetic temperature-sensing layer for artificial skins, Sci. Robot 2 (3) (2017) eaai9251.
[9] W.J. Fan, Q. He, K.Y. Meng, X.L. Tan, Z.H. Zhou, G.Q. Zhang, J. Yang, Z.L. Wang, Machine-knitted washable sensor array textile for precise epidermal physiological signal monitoring, Sci. Adv. 6 (11) (2020) eaay2840.
[10] S. Lee, A. Reuveny, J. Reeder, S. Lee, H. Jin, Q.H. Liu, T. Yokota, T. Sekitani, T. Isoyama, Y. Abe, Z.G. Suo, T. Someya, A transparent bending-insensitive pressure sensor, Nat. Nanotechnol. 11 (5) (2016) 472–478.
[11] J. Han, N. Xu, J. Yu, Y. Wang, Y. Xiong, Y. Wei, Z.L. Wang, Q. Sun, Energy Auton. Pap. Modul. Funct. Circuits Energy Environ. Sci. 15 (12) (2022) 5069–5081.
[12] M.L. Zhu, Z.D. Sun, Z.X. Zhang, Q.F. Shi, T.Y.Y. He, H.C. Liu, T. Chen, C.K. Lee, Haptic-feedback smart glove as a creative human-machine interface (HMI) for virtual/augmented reality applications, Sci. Adv. 6 (19) (2020) eaaz8693.
[13] X. Liao, W. Song, X. Zhang, C. Yan, T. Li, H. Ren, C. Liu, Y. Wang, Y. Zheng, A bioinspired analogous nerve towards artificial intelligence, Nat. Commun. 11 (1) (2020) 268.
[14] H. Jiao, X. Lin, Y. Xiong, J. Han, Y. Liu, J. Yang, S. Wu, T. Jiang, Z.L. Wang, Q. Sun, Thermal insulating textile based triboelectric nanogenerator for outdoor wearable sensing and interaction, Nano Energy 120 (2024) 109134.
[15] J. Yi, K. Dong, S. Shen, Y. Jiang, X. Peng, C.Y. Ye, Z.L. Wang, Fully fabric-based triboelectric nanogenerators as self-powered human-machine interactive keyboards, Nano-Micro Lett. 13 (1) (2021) 103.
[16] J. Ji, Z. Wang, F. Zhang, B. Wang, Y. Niu, X. Jiang, Z.-Y. Qiao, T.-l Ren, W. Zhang, S. Sang, Z. Cheng, Q. Sun, Pulse electrochemical synaptic transistor for supersensitive and ultrafast biosensors, InfoMat 5 (11) (2023) e12478.

[17] P. Zhu, H.F. Du, X.Y. Hou, P. Lu, L. Wang, J. Huang, N.N. Bai, Z.G. Wu, N.X. Fang, C.F. Guo, Skin-electrode iontronic interface for mechanosensing, Nat. Commun. 12 (1) (2021) 4731.
[18] Y. Zhang, J.L. Yang, X.Y. Hou, G. Li, L. Wang, N.N. Bai, M.K. Cai, L.Y. Zhao, Y. Wang, J.M. Zhang, K. Chen, X. Wu, C.H. Yang, Y. Dai, Z.Y. Zhang, C.F. Guo, Highly stable flexible pressure sensors with a quasi-homogeneous composition and interlinked interfaces, Nat. Commun. 13 (1) (2022).
[19] T.G. Thuruthel, B. Shih, C. Laschi, M.T. Tolley, Soft robot perception using embedded soft sensors and recurrent neural networks, Sci. Robot 4 (26) (2019) eaav1488.
[20] Y.Y. Luo, Y.Z. Li, P. Sharma, W. Shou, K. Wu, M. Foshey, B.C. Li, T. Palacios, A. Torralba, W. Matusik, Learning human-environment interactions using conformal tactile textiles, Nat. Electron 4 (3) (2021) 193–201.
[21] Y. LeCun, Y. Bengio, G. Hinton, Deep learning, Nature 521 (7553) (2015) 436–444.
[22] Z.D. Sun, M.L. Zhu, X.C. Shan, C.K. Lee, Augmented tactile-perception and haptic-feedback rings as human-machine interfaces aiming for immersive interactions, Nat. Commun. 13 (1) (2022) 5224.
[23] A. Moin, A. Zhou, A. Rahimi, A. Menon, S. Benatti, G. Alexandrov, S. Tamakloe, J. N. Ting, N. Yamamoto, Y. Khan, F. Burghardt, L. Benini, A.C. Arias, J.M. Rabaey, A wearable biosensing system with in-sensor adaptive machine learning for hand gesture recognition, Nat. Electron 4 (1) (2021) 54–63.
[24] O. Rudovic, J. Lee, M. Dai, B. Schuller, R.W. Picard, Personalized machine learning for robot perception of affect and engagement in autism therapy, Sci. Robot 3 (19) (2018) eaao6760.
[25] Z.X. Zhang, T.Y.Y. He, M.L. Zhu, Z.D. Sun, Q.F. Shi, J.X. Zhu, B.W. Dong, M. R. Yuce, C.K. Lee, Deep learning-enabled triboelectric smart socks for IoT-based gait analysis and VR applications, Npj Flex. Electron 4 (1) (2020) 29.
[26] L. Zu, J. Wen, S. Wang, M. Zhang, W. Sun, B. Chen, Z.L. Wang, Multiangle, self-powered sensor array for monitoring head impacts, Sci. Adv. 9 (20) (2023) eadg5152.
[27] Y. Lu, H. Tian, J. Cheng, F. Zhu, B. Liu, S. Wei, L. Ji, Z.L. Wang, Decoding lip language using triboelectric sensors with deep learning, Nat. Commun. 13 (1) (2022) 1401.
[28] Q.F. Shi, Z.X. Zhang, Y.Q. Yang, X.C. Shan, B. Salam, C.K. Lee, Artificial intelligence of things (AIoT) enabled floor monitoring system for smart home applications, Acs Nano 15 (11) (2021) 18312–18326.
[29] Y. Xiong, Z.W. Huo, J.T. Zhang, Y. Liu, D.W. Yue, N. Xu, R. Gu, L. Wei, L. Luo, M. X. Chen, C. Liu, Z.L. Wang, Q.J. Sun, Triboelectric in-sensor deep learning for self-powered gesture recognition toward multifunctional rescue tasks, Nano Energy 124 (2024) 109465.
[30] Z.H. Zhou, K. Chen, X.S. Li, S.L. Zhang, Y.F. Wu, Y.H. Zhou, K.Y. Meng, C.C. Sun, Q. He, W.J. Fan, E.D. Fan, Z.W. Lin, X.L. Tan, W.L. Deng, J. Yang, J. Chen, Sign-to-speech translation using machine-learning-assisted stretchable sensor arrays, Nat. Electron 3 (9) (2020) 571–578.
[31] M. Cui, H. Guo, W. Zhai, C. Liu, C. Shen, K. Dai, Template-assisted electrospun ordered hierarchical microhump arrays-based multifunctional triboelectric nanogenerator for tactile sensing and animal voice-emotion identification, Adv. Funct. Mater. 33 (46) (2023) 2301589.
[32] X. Yang, G. Liu, Q. Guo, H. Wen, R. Huang, X. Meng, J. Duan, Q. Tang, Triboelectric sensor array for internet of things based smart traffic monitoring and management system, Nano Energy 92 (2022) 106757.
[33] Z.W. Yang, Y.K. Pang, L.M. Zhang, C.X. Lu, J. Chen, T. Zhou, C. Zhang, Z.L. Wang, Tribotronic transistor array as an active tactile sensing system, ACS Nano 10 (12) (2016) 10912–10920.
[34] S. Sundaram, P. Kellnhofer, Y.Z. Li, J.Y. Zhu, A. Torralba, W. Matusik, Learning the signatures of the human grasp using a scalable tactile glove, Nature 569 (7758) (2019) 698–702.
[35] N.N. Bai, L. Wang, Q. Wang, J. Deng, Y. Wang, P. Lu, J. Huang, G. Li, Y. Zhang, J. L. Yang, K.W. Xie, X.H. Zhao, C.F. Guo, Graded intrafillable architecture-based iontronic pressure sensor with ultra-broad-range high sensitivity, Nat. Commun. 11 (1) (2020) 209.
[36] Q.F. Shi, Z.X. Zhang, T. Chen, C.K. Lee, Minimalist and multi-functional human machine interface (HMI) using a flexible wearable triboelectric patch, Nano Energy 62 (2019) 355–366.
[37] F. Wen, Z.D. Sun, T.Y.Y. He, Q.F. Shi, M.L. Zhu, Z.X. Zhang, L.H. Li, T. Zhang, C. K. Lee, Machine learning glove using self-powered conductive superhydrophobic triboelectric textile for gesture recognition in VR/AR applications, Adv. Sci. 7 (14) (2020) 2000261.
[38] S.L. Yuan, Q.X. Zeng, D.J. Tan, Y.L. Luo, X.F. Zhang, H.Y. Guo, X. Wang, Z.L. Wang, Scavenging breeze wind energy (1–8.1 ms-1) by minimalist triboelectric nanogenerator based on the wake galloping phenomenon, Nano Energy 100 (2022) 107465.
[39] C.M. Boutry, M. Negre, M. Jorda, O. Vardoulis, A. Chortos, O. Khatib, Z.N. Bao, A hierarchically patterned, bioinspired e-skin able to detect the direction of applied pressure for robotics, Sci. Robot 3 (24) (2018) eaau6914.
[40] L.Y. Xu, L. Xu, J.J. Luo, Y. Yan, B.E. Jia, X.D. Yang, Y.H. Gao, Z.L. Wang, Hybrid all-in-one power source based on high-performance spherical triboelectric nanogenerators for harvesting environmental energy, Adv. Energy Mater. 10 (36) (2020) 2001669.
[41] S. Li, N. Pan, Z.J. Zhu, R.Y. Li, B.Q. Li, J.R. Chu, G.L. Li, Y. Chang, T.R. Pan, All-in-one iontronic sensing paper, Adv. Funct. Mater. 29 (11) (2019) 1807343.
[42] F.R. Fan, Z.Q. Tian, Z.L. Wang, Flexible triboelectric generator!, Nano Energy 1 (2) (2012) 328–334.
[43] D.J. Lu, T. Liu, X.J. Meng, B. Luo, J.X. Yuan, Y.H. Liu, S. Zhang, C.C. Cai, C. Gao, J. L. Wang, S.F. Wang, S.X. Nie, Wearable triboelectric visual sensors for tactile perception, Adv. Mater. 35 (7) (2023) 2209117.
[44] L. Luo, J. Han, Y. Xiong, Z. Huo, X. Dan, J. Yu, J. Yang, L. Li, J. Sun, X. Xie, Z. L. Wang, Q. Sun, Kirigami interactive triboelectric mechanologic, Nano Energy 99 (2022) 107345.
[45] H.L. Zhang, Y. Yang, Y.J. Su, J. Chen, K. Adams, S. Lee, C.G. Hu, Z.L. Wang, Triboelectric nanogenerator for harvesting vibration energy in full space and as self- powered acceleration sensor, Adv. Funct. Mater. 24 (10) (2014) 1401–1407.
[46] K.Q. Xia, J.M. Fu, Z.W. Xu, Multiple-frequency high-output triboelectric nanogenerator based on a water balloon for all-weather water wave energy harvesting, Adv. Energy Mater. 10 (28) (2020) 2000426.
[47] K.Q. Xia, H.C. Tang, J.M. Fu, Y. Tian, Z.W. Xu, J.G. Lu, Z.Y. Zhu, A high strength triboelectric nanogenerator based on rigid-flexible coupling design for energy storage system, Nano Energy 67 (2020) 104259.
[48] Z.Y. Che, X. Wan, J. Xu, C. Duan, T.Q. Zheng, J. Chen, Speaking without vocal folds using a machine-learning-assisted wearable sensing-actuation system, Nat. Commun. 15 (1) (2024) 1873.
[49] C. Chen, Z. Wen, J. Shi, X. Jian, P. Li, J.T.W. Yeow, X. Sun, Micro triboelectric ultrasonic device for acoustic energy transfer and signal communication, Nat. Commun. 11 (1) (2020) 4143.
[50] Q.F. Shi, H. Wu, H. Wang, H.X. Wu, C.K. Lee, Self-powered gyroscope ball using a triboelectric mechanism, Adv. Energy Mater. 7 (22) (2017) 1701300.
[51] Y. Xiong, L. Luo, J.H. Yang, J. Han, Y. Liu, H.S. Jiao, S.S. Wu, L.Q. Cheng, Z. Y. Feng, J. Sun, Z.L. Wang, Q.J. Sun, Scalable spinning, winding, and knitting graphene textile TENG for energy harvesting and human motion recognition, Nano Energy 107 (2023) 108137.
[52] J.R. Yu, X.X. Yang, G.Y. Gao, Y. Xiong, Y.F. Wang, J. Han, Y.H. Chen, H. Zhang, Q. J. Sun, Z.L. Wang, Bioinspired mechano-photonic artificial synapse based on graphene/MoS_2 heterostructure, Sci. Adv. 7 (12) (2021) eabd9117.
[53] C.J. Wan, G. Chen, Y.M. Fu, M. Wang, N. Matsuhisa, S.W. Pan, L. Pan, H. Yang, Q. Wan, L.Q. Zhu, X.D. Chen, An artificial sensory neuron with tactile perceptual learning, Adv. Mater. 30 (30) (2018) 1801291.
[54] G.Z. Li, S.Q. Liu, L.Q. Wang, R. Zhu, Skin-inspired quadruple tactile sensors integrated on a robot hand enable object recognition, Sci. Robot 5 (49) (2020) eabc8134.
[55] T. Jin, Z.D. Sun, L. Li, Q. Zhang, M.L. Zhu, Z.X. Zhang, G.J. Yuan, T. Chen, Y. Z. Tian, X.Y. Hou, C. Lee, Triboelectric nanogenerator sensors for soft robotics aiming at digital twin applications, Nat. Commun. 11 (1) (2020) 5381.
[56] C.B. Zhuang, J.H. Liu, H. Xiong, Digital twin-based smart production management and control framework for the complex product assembly shop-floor, Int J. Adv. Manuf. Tech. 96 (1-4) (2018) 1149–1163.
[57] S. Seo, T. Kim, H.H. Lee, Simple fabrication of nanostructure by continuous rigiflex imprinting, Mircoelectron Eng. 84 (4) (2007) 567–572.
[58] H.Y. Guo, X.J. Pu, J. Chen, Y. Meng, M.H. Yeh, G.L. Liu, Q. Tang, B.D. Chen, D. Liu, S. Qi, C.S. Wu, C.G. Hu, J. Wang, Z.L. Wang, A highly sensitive, self-powered triboelectric auditory sensor for social robotics and hearing aids, Sci. Robot 3 (20) (2018) eaat2516.
[59] C.S. Wu, W.B. Ding, R.Y. Liu, J.Y. Wang, A.C. Wang, J. Wang, S.M. Li, Y.L. Zi, Z. L. Wang, Keystroke dynamics enabled authentication and identification using triboelectric nanogenerator array, Mater. Today 21 (3) (2018) 216–222.

Yao Xiong received her bachelor's degree from University of Science and Technology Beijing in 2019. Now she is a doctor candidate in Beijing Institute of Nanoenergy and Nanosystems, Chinese Academy of Sciences. Her research direction mainly includes energy harvesting, self-fpowered sensors and corresponding intelligent application.

Yang Liu received her master's degree from Guangxi University in 2023. Now she is a doctor candidate in Beijing Institute of Nanoenergy and Nanosystems, Chinese Academy of Sciences. Her main research direction mainly focuses on self-powered sensors and corresponding intelligent applications.

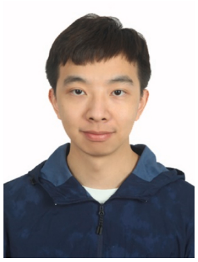

Jiahong Yang received the Master's degree from Guangxi University in 2022. Now, he is a PhD candidate at the Institute of Nanoenergy and Nanosystems, Chinese Academy of Sciences, Beijing, China. His research interests mainly include self-driven sensors, liquid metals and friction electric harvesting systems.

Yifei Wang received his B.S. degree from China University of Geosciences (Beijing) in 2018. He is pursuing his Ph.D. under the supervision of Professor Qijun Sun at Beijing Institute of Nanoenergy and Nanosystems, Chinese Academy of Sciences, University of Chinese Academy of Sciences. His research interests are focused on self-powered sensors and triboelectricity activated neuromorphic devices.

Nuo Xu received her B.S. degree from South China University in 2017. She is now a PhD student in the School of Physical Science and Engineering Technology, Guangxi University, where she is co-trained at the Institute of Nanoenergy and Nanosystems, Beijing, under the supervision of Prof. Qijun Sun. Her research focuses on the study of paper-based electronic circuits and their neuromorphic devices.

Prof. Zhong Lin Wang received his Ph. D from Arizona State University in physics. He now is the Hightower Chair in Materials Science and Engineering, Regents' Professor, Engineering Distinguished Professor and Director, Center for Nanostructure Characterization, at Georgia Tech. Dr. Wang has made original and innovative contributions to the synthesis, discovery, characterization and understanding of fundamental physical properties of oxide nanobelts and nanowires, as well as applications of nanowires in energy sciences, electronics, optoelectronics and biological science. He pioneered the field of piezotronics and piezo-phototronics by introducing piezoelectric potential gated charge transport process in fabricating new electronic and optoelectronic devices.

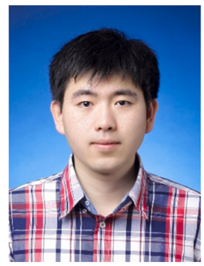

Prof. Qijun Sun has joined Beijing Institute of Nanoenergy and Nanosystems (CAS) since 2016, as the principal investigator of Functional Soft Electronics Lab. The main research interests of his group include triboiontronic devices, mechanoplastic neuromorphic transistors, artificial synaptic devices electronic skin, 2D materials based flexible semiconductor devices, human-machine interactive systems and micro-nano fabrication, aiming to develop advanced systems for human health monitoring and human-robotic interface.